

COMPARISON OF PRECIPITATION EFFECTS IN SPACE-BORNE X- AND KA-BAND SAR IMAGING

A. Danklmayer

German Aerospace Center (DLR)
Microwaves and Radar Institute
Oberpfaffenhofen, Germany

M. Chandra

Chemnitz University of Technology
Dept. of Microwave Eng. and Photonics
Chemnitz, Germany

ABSTRACT

As the operating frequencies of SAR-systems are increasing, the visible distortions due to precipitation in SAR-images are becoming more frequent. This holds especially for the case of convective rain events. The German space-borne satellite TerraSAR-X has delivered a series of measurement examples, which were used to study precipitation effects in SAR-images. Based on these valuable data takes and simultaneous weather radar measurements, a quantitative estimation of precipitation effects in SAR-images is presented. In a further step, an attempt is made to extrapolate the observed effects to systems operating at higher nominal frequency-bands, i.e. Ka-band, being taken under consideration for future SAR-systems.

Index Terms— Synthetic-aperture radar (SAR), Microwave imaging, Propagation effects, Signal attenuation, Precipitation

1. INTRODUCTION

Since 2007, TerraSAR-X is ready to deliver outstanding data, day and night, and during almost all weather conditions. Microwave SAR imaging at X-band frequencies is sometimes affected by propagation effects due to heavy rain, as can be seen in Fig. 1. The physical processes involved are

- reflection at the precipitation volume
- attenuation through the precipitation volume
- change of the surface due to the wetness and for water-surfaces due to the impinging rain drops or due to the influence by the wind

Today, a considerable body of literature exists on propagation effects in SAR imaging and how to make use of SAR data to deduce meteorological information [1][2][3].

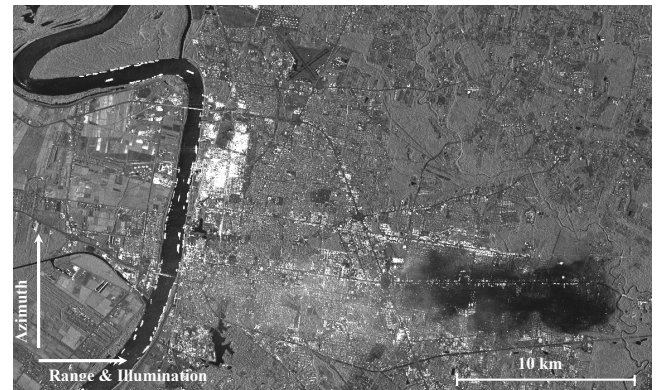


Fig. 1. An example of a SAR image with rain-cell signatures recorded with TerraSAR-X in the US close to Baton Rouge. The white shading is due to direct reflections from the rain region (shown as volume 'A' in Fig. 2). Whereas the darkly shaded areas are due to rain attenuated (blocked) signals from the ground; this effect is shown as region 'B' in Fig. 2.

2. ANALYSIS OF DATASETS AND PHYSICAL INTERPRETATION OF ARTEFACTS IN SAR IMAGES DUE TO PRECIPITATION

A physical interpretation of how rain cells affect SAR images is shown in Fig. 2. The sketch shows an imaging scenario, where the transmitted waves interact with a precipitation cell. It can be observed that area 'A', which corresponds to time instant τ_A in the amplitude/time diagram, is due to strong backscattering from large hydrometeors. Time instant τ_B , which corresponds to the region 'B' proves that signals have been heavily attenuated. By comparing the dark patch in Fig. 1 and the amplitude/time diagram in Fig. 2, the veil in Fig. 1 corresponds to area 'A' (τ_A), and the shadowlike black areas close to this veil in Fig. 1 corresponds to the region 'B' (τ_B) in Fig. 2.

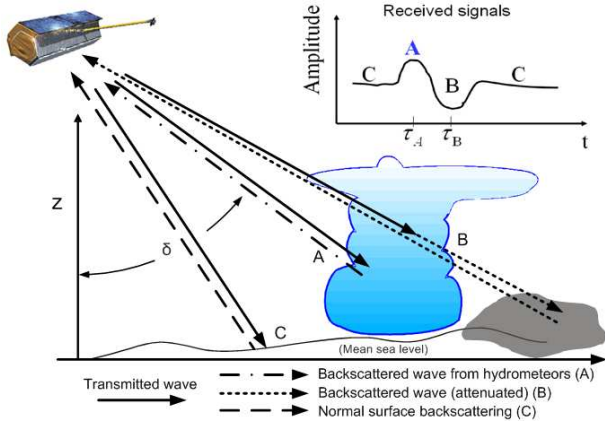


Fig. 2. A physical interpretation of rain cell signatures in SAR-images, as indicated and introduced previously in Fig. 1.

2.1. Attenuation through rain

One of the major problems affecting microwave and millimetre wave bands for terrestrial and space-borne radars is the attenuation through rain [4, 5]. A convenient way to describe the rain intensity is the so called rainfall-rate or rain-rate given in millimetres per hour. This quantity refers to a certain flux of rain towards the surface of the Earth and may be measured e.g. by gauges or weather radars. A widely accepted empirical relation of the form

$$\gamma(x, t) = a \cdot R^b \quad (1)$$

between specific attenuation $\gamma(x, t)$ and rain rate R is used to calculate the specific attenuation for a given rain rate [4, 6]. The parameters a and b are dependent on the radio frequency, the raindrop size distribution, the polarization and other factors [6].

After [4], the total attenuation for a given instant of time can be obtained by adding up the specific attenuation along the path of propagation using the following expression

$$A(t) = \int_0^{2h} \gamma(x, t) dx \quad (2)$$

where

$A(t)$... total attenuation for given time instant t
t	... time
h	... path length
$\gamma(x, t)$... specific attenuation
x	... position along the path of propagation

The specific attenuation along the slant path of propagation has to be known. However, detailed knowledge of the medium through which the signal propagates is rather limited and the temporal and spatial variation of the medium require assumptions and some modelling [7]. In the case of precipitation we may have some idea about the thermodynamic phase

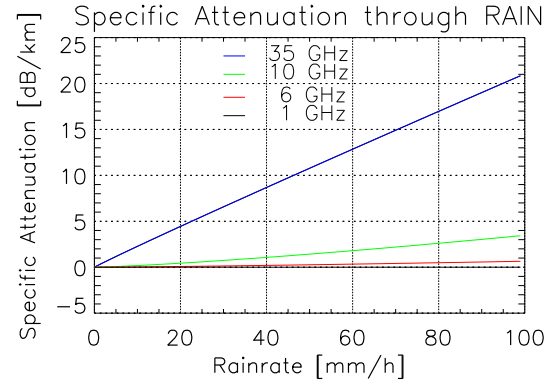


Fig. 3. A plot of the specific attenuation given in units of dB/km versus the rain rate in units of mm/hr for four different frequencies (1, 6, 10 and 35 GHz) after the ITU Model Recommendation 838 (1994).

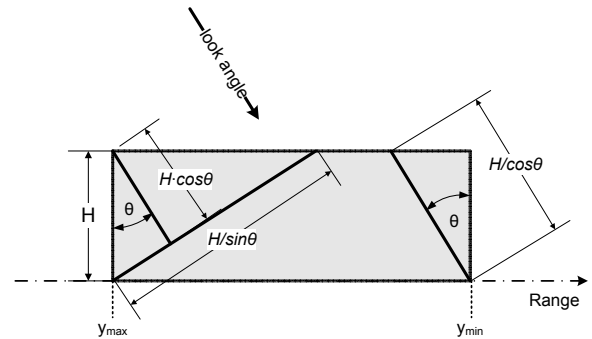


Fig. 4. The structure of an idealised rain cell used for the calculation in Section 2.2.

(ice, water, melting band) but no precise information. Using the calculated values for the specific attenuation in X-band provided in diagram Fig.3 for a 5 km long path through a heavy tropical convective rain (70 mm/hr and more) suggests a 20 – 30 dB attenuation, which was confirmed by comparing the backscattering coefficient of affected and non-affected region from data takes acquired by TerraSAR-X over Brazilian rain forest.

2.2. Modelling of the Attenuation under Rain Conditions for X-band and Ka-band

For the calculations of the rain rate to cause visible attenuation in Ka-band SAR images, a simple model shown in Fig. 4 [8], is used. A reasonable height of 4 km is assumed, as well as a homogenous rain rate for the modelled cell. The incidence angle of the propagating signals was chosen 30° . With the help of (1) and by using the regression coefficients in Table 1, the specific attenuation was calculated. These values are given in Table 2. Finally, the values for the two-way path attenuation for different rain rates (5, 50 and 100 mm/hr) can

Table 1. Regression coefficients used in (1) and (4)

Frequency	DSD			
	Marshall Pallmer a	b	Joss Thunderstorm a	b
X-band (10 GHz)	0.0136	1.15	0.0169	1.076
Ka-band (35 GHz)	0.268	1.007	0.372	0.783

be found in Table 3. As a total two-way attenuation of 25 dB becomes visible in SAR images in X-band it is of interest which rain rate is necessary to cause such an attenuation for Ka-band (35 GHz) frequencies. To this end, the following equation is applied

$$\gamma(t) = \frac{A(t)}{2 \cdot \frac{H}{\cos(\theta)}} \quad [\text{dB/km}] \quad (3)$$

where the rain rate is found using (1) with the according parameters a and b for Ka-band.

$$R = \sqrt[b]{\frac{\gamma(t)}{a}} \quad [\text{mm/h}] \quad (4)$$

First calculations using the parameters of the idealised rain cell of 4 km and using 25 dB of total two-way attenuation, assuming the Marshall Pallmer Parameters for Ka-band attenuation deliver a rain rate close to 10 mm/hr. This simple example demonstrates that such rain rates are fully capable to distort Ka-band SAR measurements to a visible extent. In Fig. 5 the range of values for attenuation and rain rate are extended and the diagram shows the two-way attenuation versus the rain rate for different incidence angles at Ka-band. Similar information is provided for X-band frequencies in Fig. 6. The simple assumptions of a homogenous rain cell with constant precipitation may be somehow optimistic, since a melting layer precipitation may severely increase the total path attenuation.

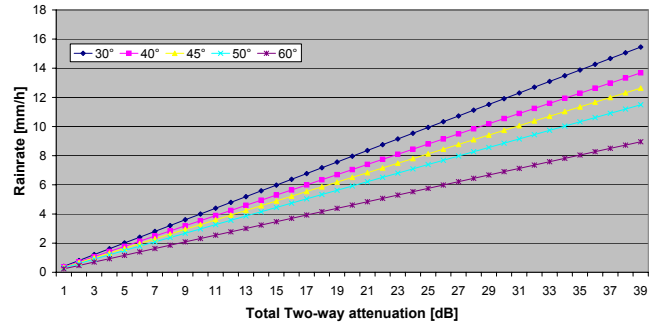
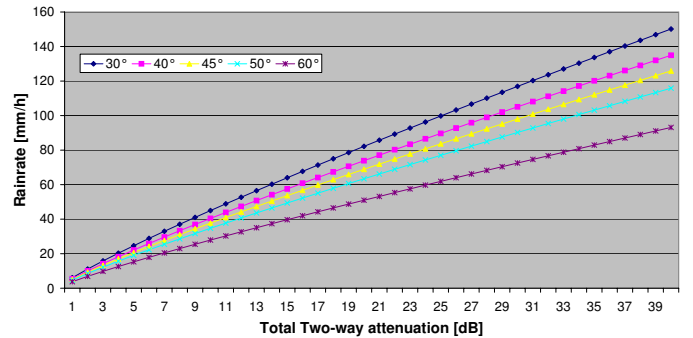
A test case close to New Orleans, US is provided in Fig. 7 and was selected to perform a comparison between two different types of measurements (left: TerraSAR-X; middle: NOAA ground-based weather radar data) and one artificially generated product (right) based on the modeling approach shown above. The two almost isolated rain cells with reflectivities of up to 50 dBZ, depicted in the weatherradar image (middle), are ideally suited to be used for extrapolation and modeling of respective attenuation and backscattering effects for Ka-band. As expected, the attenuation due to rain increases dramatically at Ka-band and therefore the visible artefacts are more pronounced but limited to regions where the rain rate is about 10 mm/hr. The backscattering at Ka-band due to rain is also increased compared to X-band which results in zones of bright veils appearing to the left of the precipitation cells (in the direction towards the radar).

Table 2. Specific Attenuation [dB/km]

Rainrate [mm/hr]	Specific Attenuation	
	10 GHz	35 GHz
5	0.08	1.31
50	1.22	7.95
100	2.4	13.69

Table 3. Maximum Attenuation for modelled rain cell [dB]

Rainrate [mm/hr]	Specific Attenuation	
	10 GHz	35 GHz
5	0.739	12.1
50	11.26	73.43
100	22.17	126.46

**Fig. 5.** A diagram of the two-way path attenuation and the corresponding rain rate for the modelled rain cell of 4 km height (Fig. 4) at Ka-band (35 GHz), for different look angles.**Fig. 6.** A diagram of the two-way path attenuation and the corresponding rain rate for the modelled rain cell (Fig. 4) at X-band (10 GHz), for different look angles.

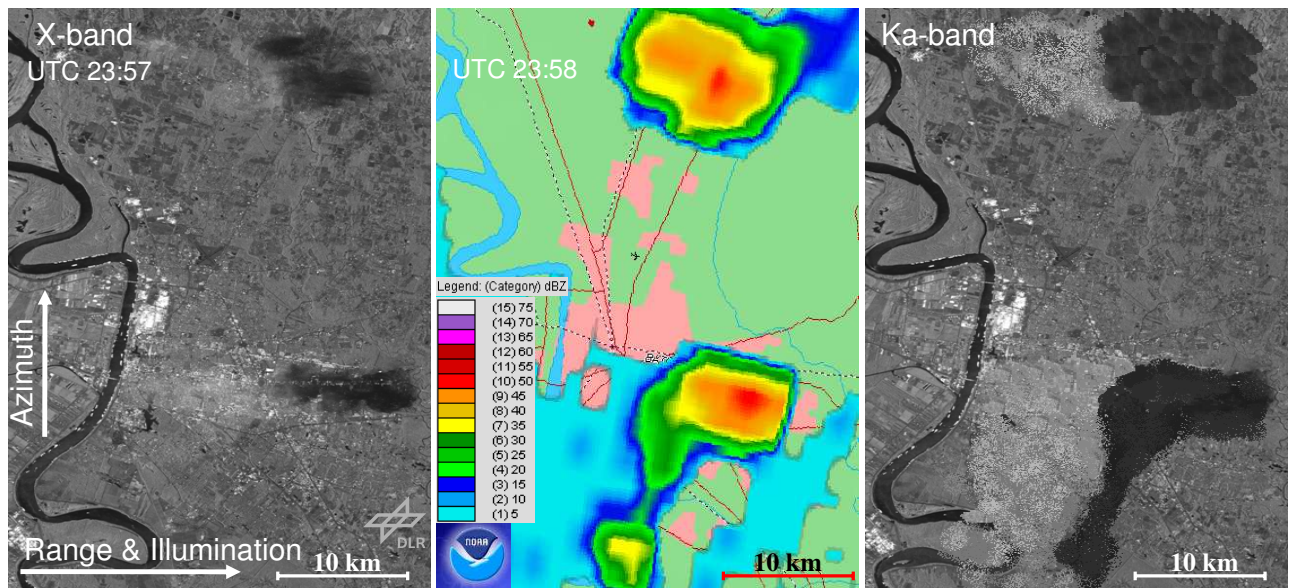


Fig. 7. Depiction and comparison of three different kinds of datasets. In the middle a weather radar image is given, showing a reflectivity map of two almost isolated raincells with reflectivity values up to 50 dBZ. To the left a corresponding SAR image measured with TerraSAR-X is provided. Signatures due to precipitation can be clearly identified. To the right, an artificially generated image based on TerraSAR-X data is given and it shows how artefacts at Ka-band may look like. The estimation of the attenuation is based on the modelling provided in Section 2.2.

3. CONCLUSIONS

As well known, attenuation due to rain is the dominating effect when considering propagation effects in SAR imaging at higher frequency bands such as X- and Ka-band. For the case of TerraSAR-X only convective precipitation events have the potential to generate visible artefacts in SAR images. For the Ka-band rain rates of 10 mm/h are capable to produce visible artefacts.

Acknowledgements

This research was partly financed by ESA under contract No. 21876/08/NL/ST/al "Precipitation effects for Ka-band SAR". A. Danklmayer would like to sincerely thank Dipl.-Ing. Patrick Tracksdorf for proofreading of the paper.

4. REFERENCES

- [1] A. Danklmayer, "Propagation effects and polarimetric methods in synthetic aperture radar (SAR) imaging," Ph.D. dissertation, Chemnitz University of Technology, DLR-Report FB-2008-14, Technical University of Chemnitz, 2008.
- [2] A. Danklmayer and M. Chandra, "Precipitation induced signatures in SAR images," in *Proceedings of European Conference on Antennas and Propagation (EuCAP) 2009*, Berlin, Germany, 3 2009.
- [3] A. Danklmayer, B. Döring, M. Schwerdt, and M. Chandra, "Assessment of Atmospheric Effects in SAR Images," *IEEE Transaction on Geoscience and Remote Sensing*, 2009, accepted for publication.
- [4] R. K. Crane, *Electromagnetic wave propagation through rain*. John Wiley and Sons, 1996.
- [5] P. Ferrazzoli and G. Schiavon, "Rain-induced modification of SAR performance," *Adv. Space Res.*, vol. 7, no. 11, pp. 269–272, 1987.
- [6] R. L. Olsen, D. V. Rogers, and D. B. Hodge, "The $a \cdot R^b$ relation in calculation of rain attenuation," *IEEE Transactions on Antennas and Propagation*, vol. 26, no. 2, pp. 318–329, 1978.
- [7] A. W. Doerry, "Atmospheric loss considerations for synthetic aperture radar design and operation," in *Proceedings of SPIE*, 2004.
- [8] C. Melsheimer, *Signaturen von Regen in Radaraufnahmen des Meeres*. Aachen: Shaker Verlag, 1998.